Electronic Supplementary Information (ESI)

Aggregation of nitroaniline in tetrahydrofuran through intriguing H-Bond formation by sodium borohydride

Mainak Ganguly,[a] Chanchal Mondal,[a] Anjali Pal,[b] Saied Md Pratik,[c] Jaya Pal,[a] and Tarasankar Pal*[a]

[a]Department of Chemistry, Indian Institute of Technology, Kharagpur-721302, West Bengal, India

[b]Department of Civil Engineering, Indian Institute of Technology, West Bengal, Kharagpur-721302, India

[c]Department of Spectroscopy, Indian Association for the Cultivation of Science, Jadavpur – 700032, West Bengal, India

E-mail: tpal@chem.iitkgp.ernet.in

Computational Details

Contents

1. Cartesian coordinates for the optimized structures and their zero point energy corrected total energies in Hartree and low vibrational frequencies in cm^{-1}.

All the structures were optimized using the M0-62X/6-31+G(d,p) level of theory in tetrahydrofuran (THF) modeled using IEFPCM method. The harmonic frequencies were calculated at 298K.

2. Complete Reference for Gaussian 09.

(a) P-NA

Atomic	**Coordinates (Angstroms)**		
Number	**X**	**Y**	**Z**
6	0.000000	0.706556	0.000000
6	0.000000	0.022557	1.217031
6	0.000000	-1.358746	1.216290
6	0.000000	-2.076573	0.000000
6	0.000000	-1.358746	-1.216290
6	0.000000	0.022557	-1.217031
1	0.000000	0.577435	2.147520
1	0.000000	-1.900878	2.156588
1	0.000000	-1.900878	-2.156588

1	0.000000	0.577435	-2.147520
7	-0.036577	-3.440241	0.000000
7	0.000000	2.152978	0.000000
1	0.161871	-3.938357	-0.854156
1	0.161871	-3.938357	0.854156
8	0.000000	2.736801	-1.077809
8	0.000000	2.736801	1.077809

Energy = -491.821955 Hartree

Low frequencies (cm^{-1}): 61.8582 113.3617 230.6870

289.0683 296.3525 371.3412

395.9361 420.4227 447.8840

(b) <u>DMR</u>

Atomic	Coordinates (Angstroms)		
Number	X	Y	Z
6	4.729512	1.206207	0.171531

6	3.402962	1.570750	0.070530
6	2.392952	0.588838	-0.075610
6	2.772873	-0.775136	-0.117033
6	4.099490	-1.138598	-0.016710
6	5.075742	-0.147593	0.127566
1	5.503421	1.955980	0.285304
1	3.124266	2.619295	0.103043
1	2.007013	-1.535758	-0.230539
1	4.393166	-2.181143	-0.047854
6	-4.569250	1.166486	-0.066198
6	-5.927173	0.941471	0.018430
6	-6.437620	-0.377462	0.051234
6	-5.531631	-1.462499	0.000000
6	-4.173273	-1.238155	-0.090995
6	-3.696288	0.075748	-0.120794
1	-4.174652	2.175162	-0.091802
1	-6.614246	1.780081	0.061087
1	-5.912576	-2.478185	0.021019
1	-3.475787	-2.065992	-0.135001
7	-7.772297	-0.596859	0.156936
7	-2.281259	0.312674	-0.208865
7	1.092040	0.940768	-0.181171
7	6.461198	-0.528207	0.234512
1	-8.147898	-1.527957	0.069450
1	-8.424068	0.169086	0.091304

1	0.351350	0.253192	-0.239832
1	0.803707	1.904158	-0.115070
8	-1.522666	-0.656338	-0.265585
8	-1.873178	1.469357	-0.223616
8	6.746549	-1.721572	0.195825
8	7.304139	0.355190	0.360718

Energy = -983.650524 Hartree

Low frequencies (cm^{-1}): 10.5962 16.4874 18.5795

28.3938 51.1236 71.6870

74.5169 80.8870 111.6436

112.3005 175.5990 234.8174

2. Complete Reference for Gaussian 09: Gaussian 09, Frisch, M. J.; Trucks, G. W.; Schlegel, H. B.; Scuseria, G.

E.; Robb, M. A.; Cheeseman, J. R.; Scalmani, G.; Barone, V.; Mennucci, B.; Petersson, G. A.; Nakatsuji, H.; Caricato, M.;

Li, X.; Hratchian, H. P.; Izmaylov, A. F.; Bloino, J.; Zheng, G.; Sonnenberg, J. L.; Hada, M.; Ehara, M.; Toyota, K.;

Fukuda, R.; Hasegawa, J.; Ishida, M.; Nakajima, T.; Honda, Y.; Kitao, O.; Nakai, H.; Vreven, T.; Montgomery, Jr., J. A.;

Peralta, J. E.; Ogliaro, F.; Bearpark, M.; Heyd, J. J.; Brothers, E.; Kudin, K. N.; Staroverov, V. N.; Kobayashi, R.;

Normand, J.; Raghavachari, K.; Rendell, A.; Burant, J. C.; Iyengar, S. S.; Tomasi, J.; Cossi, M.; Rega, N.; Millam, N. J.;

Klene, M.; Knox, J. E.; Cross, J. B.; Bakken, V.; Adamo, C.; Jaramillo, J.; Gomperts, R.; Stratmann, R. E.; Yazyev, O.;

Austin, A. J.; Cammi, R.; Pomelli, C.; Ochterski, J. W.; Martin, R. L.; Morokuma, K.; Zakrzewski, V. G.; Voth, G. A.;

Salvador, P.; Dannenberg, J. J.; Dapprich, S.; Daniels, A. D.; Farkas, Ö.; Foresman, J. B.; Ortiz, J. V.; Cioslowski, J.; Fox,

D. J. Gaussian, Inc., Wallingford CT, 2009.

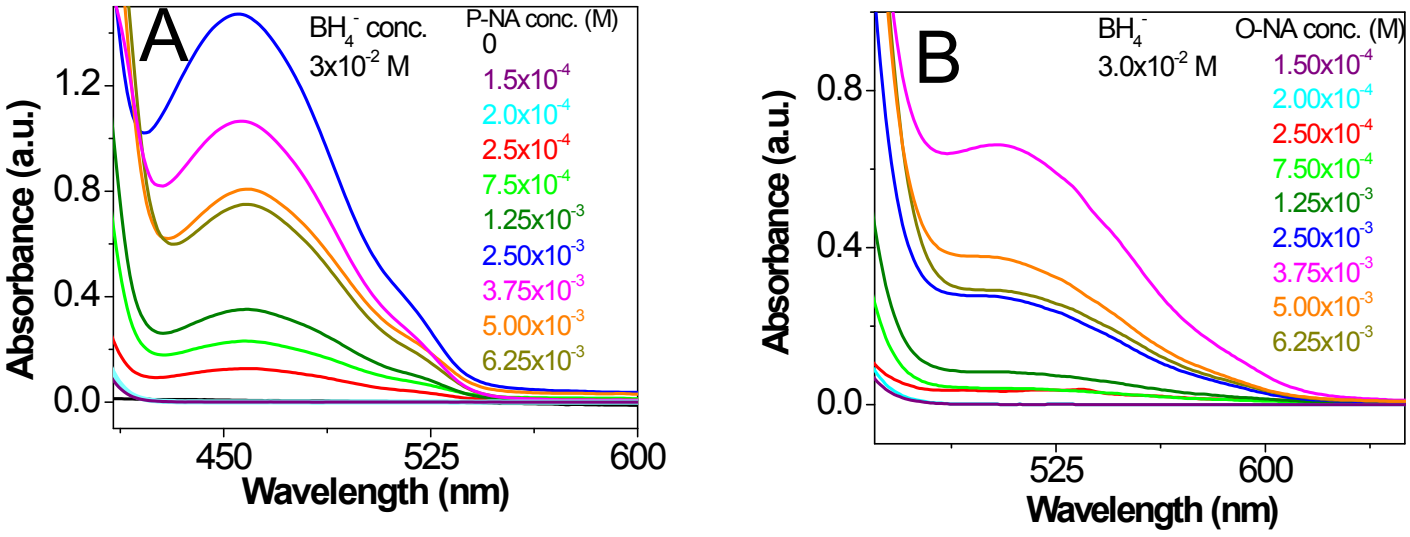

Figure S1: Absorption spectral profile when (A) BH_4^- concentration is fixed and P-NA concentration is variable, (B) BH_4^- concentration is fixed and O-NA concentration is variable. For P-NA, absorption peak maximum of 458 nm has been considered and for O-NA, absorption peak maximum of 500 nm has been considered.

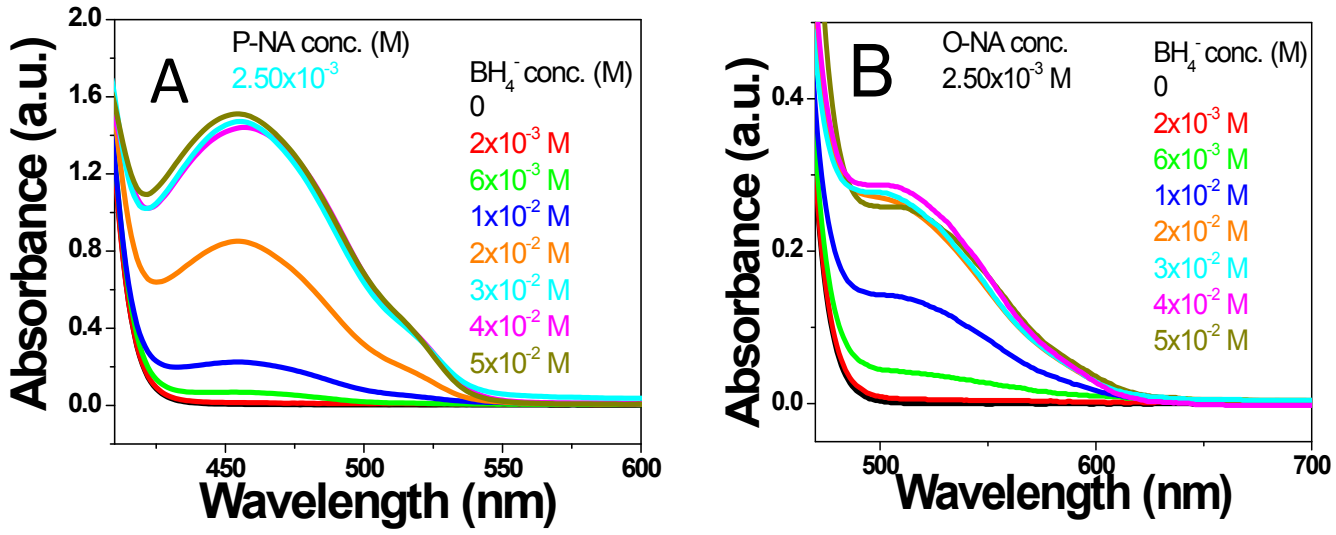

Figure S2: Absorption spectral profile when (A) BH_4^- concentration is variable and P-NA concentration is fixed, (B) BH_4^- concentration is variable and O-NA concentration is fixed. For P-NA, absorption peak maximum of 458 nm has been considered and for O-NA, absorption peak maximum of 500 nm has been considered.

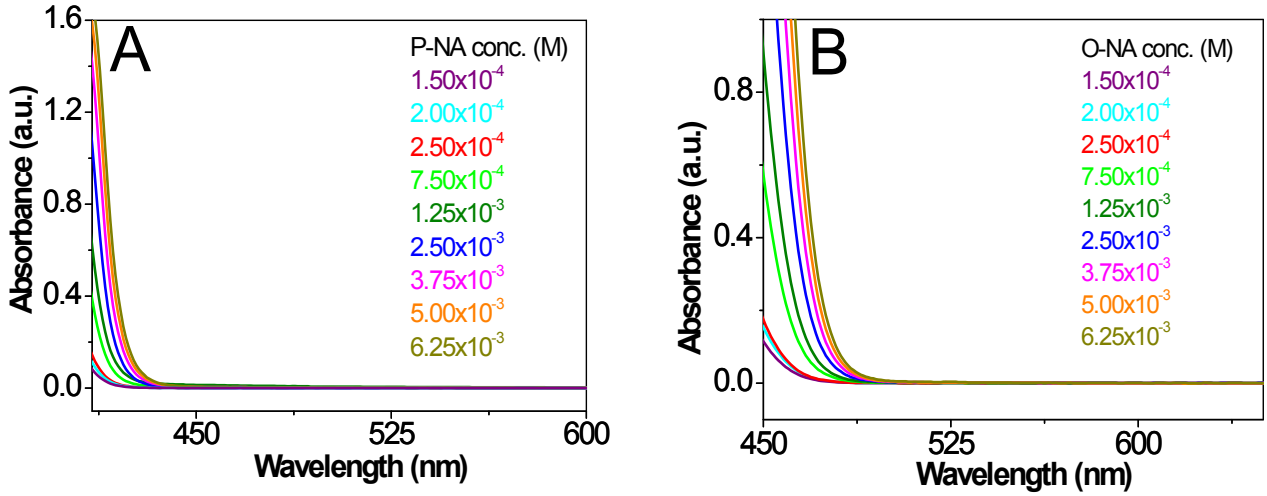

Figure S3: Absorption spectral profile of (A) P-NA 1 and (B) O-NA 2 at various NA concentrations.

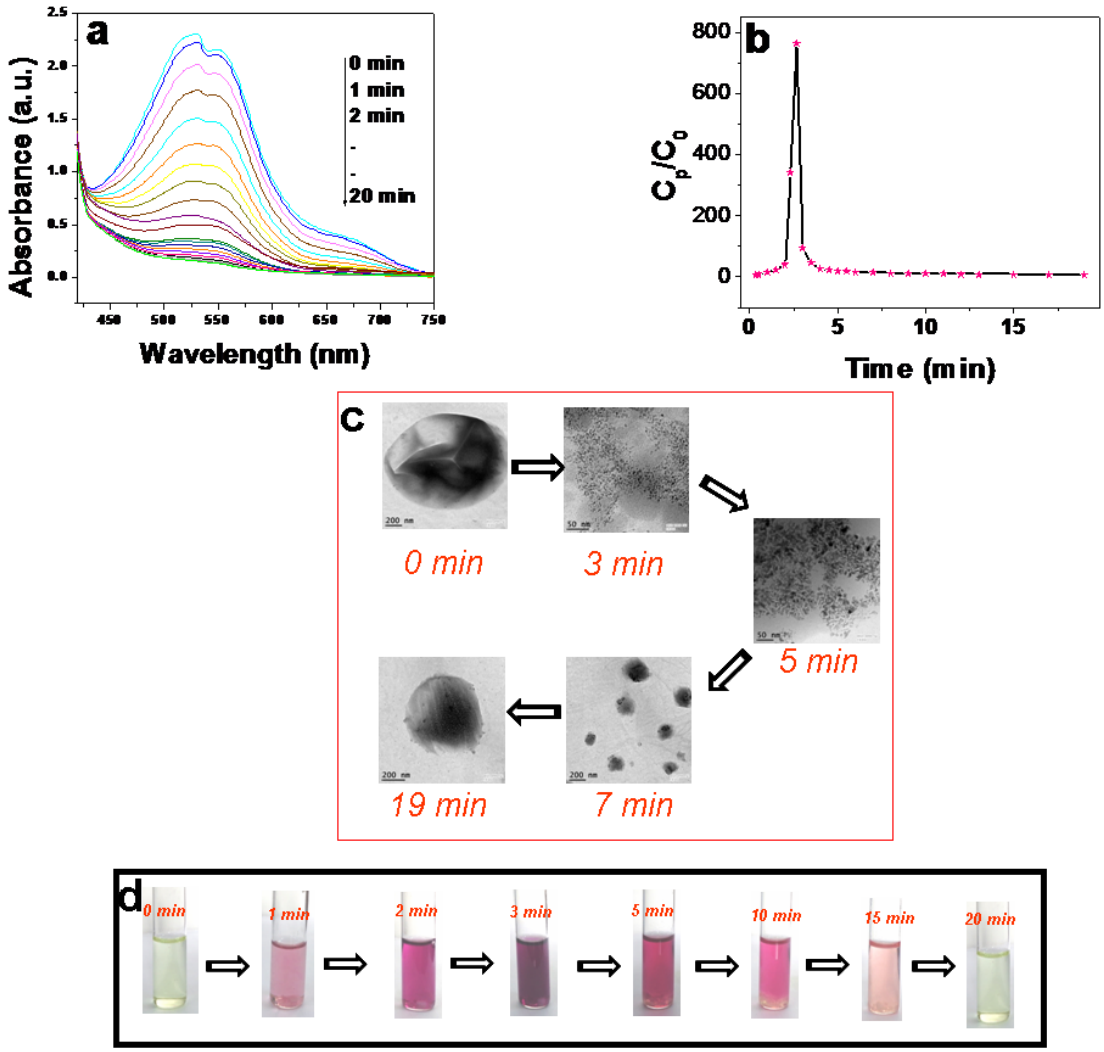

Figure S4: (a) UV-visible spectra showing the kinetics of destruction of anion radical of nitrobenzene in THF (nitrobenzene conc. = 0.97 M, $NaBH_4$ = 15 mg). (b) Plot showing the change in capacitance of nitrobenzene anion radical in THF with time. (c) TEM images to show the fate of nitrobenzene (0.97 M) at different time interval after borohydride (15 mg) addition in THF. (d) Digital image to show the evolution and destruction of anion radical of 0.97 M nitrobenzene in THF with time in presence of borohydride (15 mg).

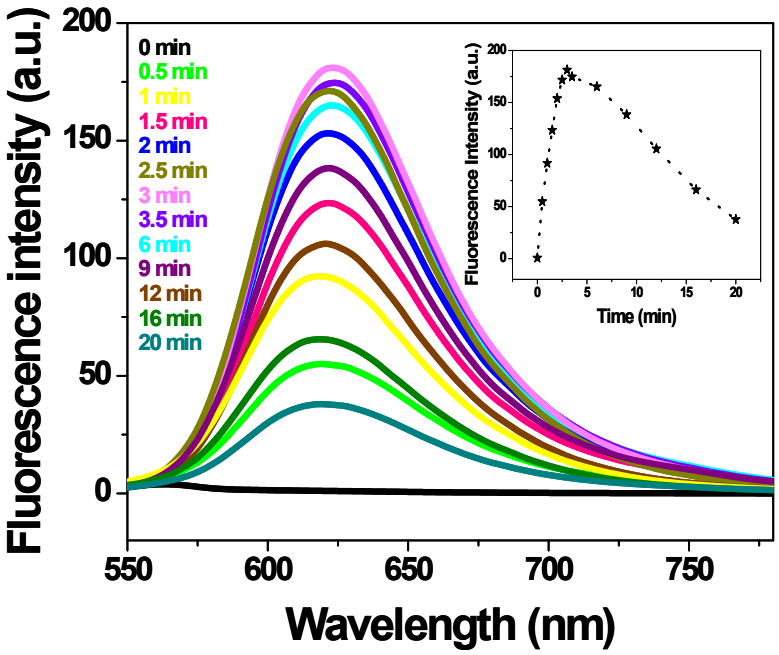

Figure S5: Fluorescence spectra showing the evolution and destruction of anion radical of nitrobenzene with time.

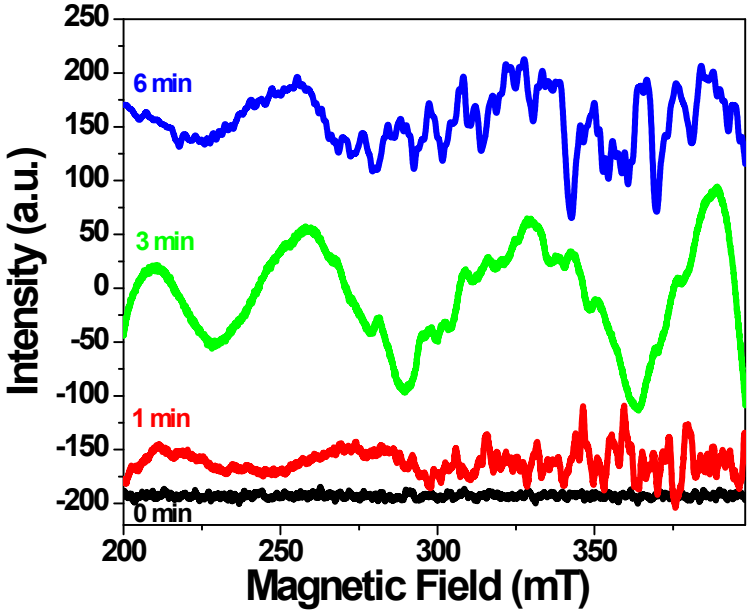

Figure S6: EPR spectra showing the evolution and destruction of anion radical of nitrobenzene with time. After 3 min, formation of anion radical becomes maximum [d = 3.1 (210 mT), 2.5 (259 mT) and 1.93 (329 mT)].

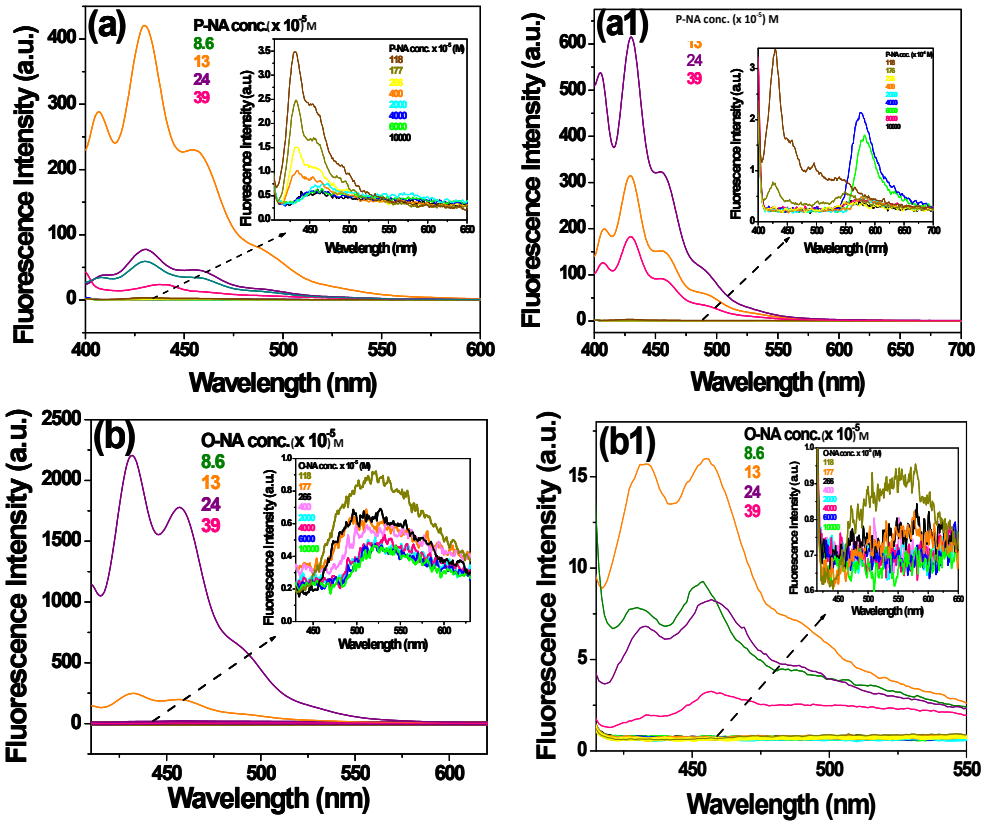

Figure S7: Fluorescence spectra of (a) P-NA 1 (λ_{ex}=390 nm), (a1) P-NA 2 (λ_{ex}=390 nm), (b) O-NA 1 (λ_{ex}=400 nm) and (b2) O-NA 2 (λ_{ex}=400 nm) at different nitroaniline concentrations; $NaBH_4$ used =15 mg.

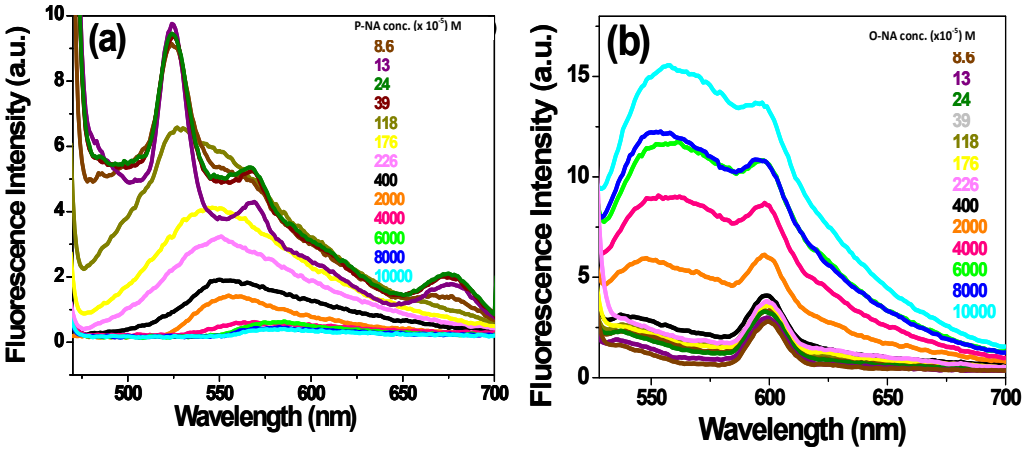

Figure S8: Fluorescence spectra of (a) P-NA 2 (λ_{ex}=458 nm) and (b) O-NA 2 (λ_{ex}=500 nm) at different nitroaniline concentrations; $NaBH_4$ used =15 mg.

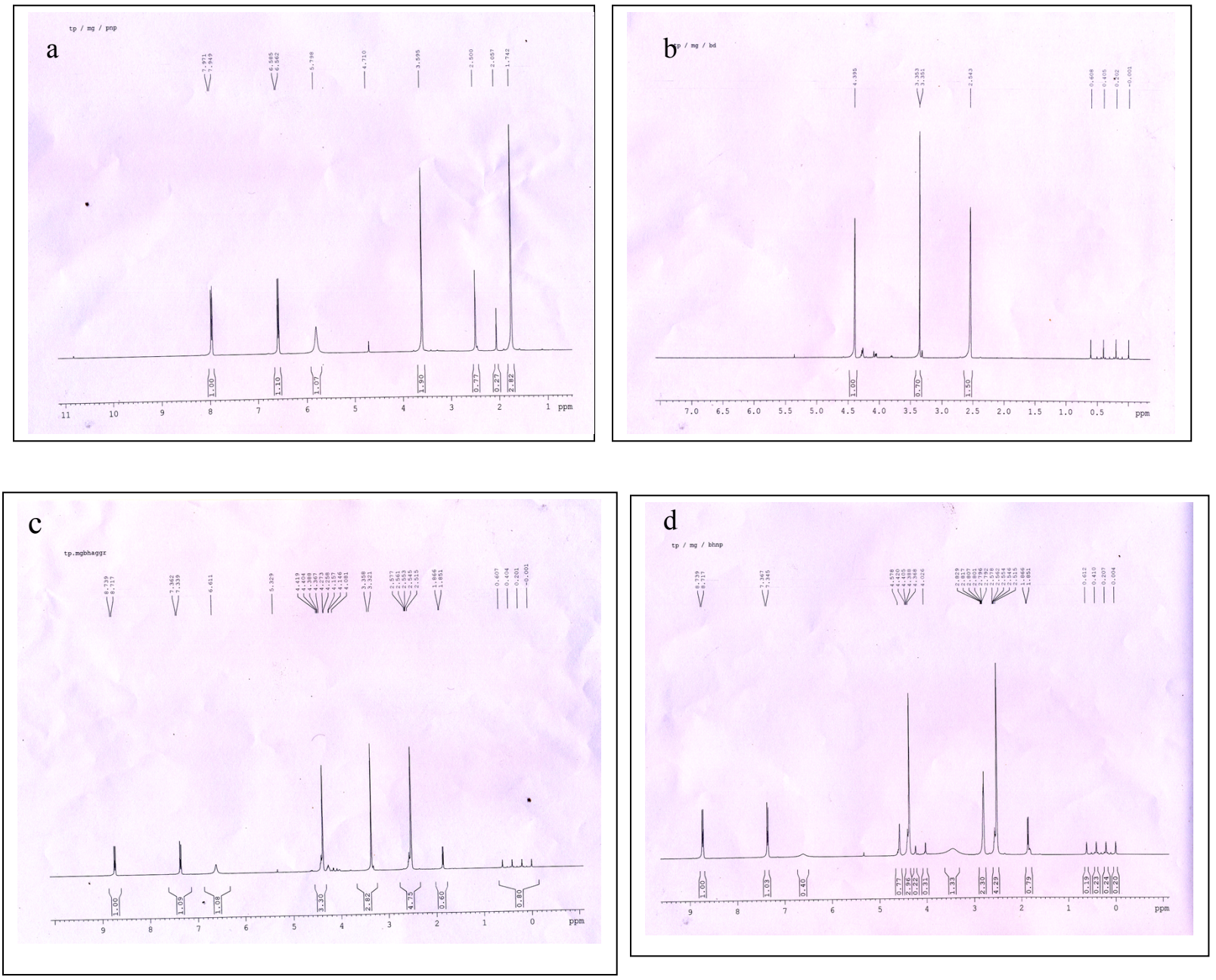

Figure S9: ^{1}H-NMR of (a) P-NA 1 in d^{8}-THF, (b) d^{8}-THF + $NaBH_4$, (c) P-NA 2 in d^{8}-THF and (d) P-NA 3 (P-NA 2 + d^{6}-acetone) in d^{8}-THF.

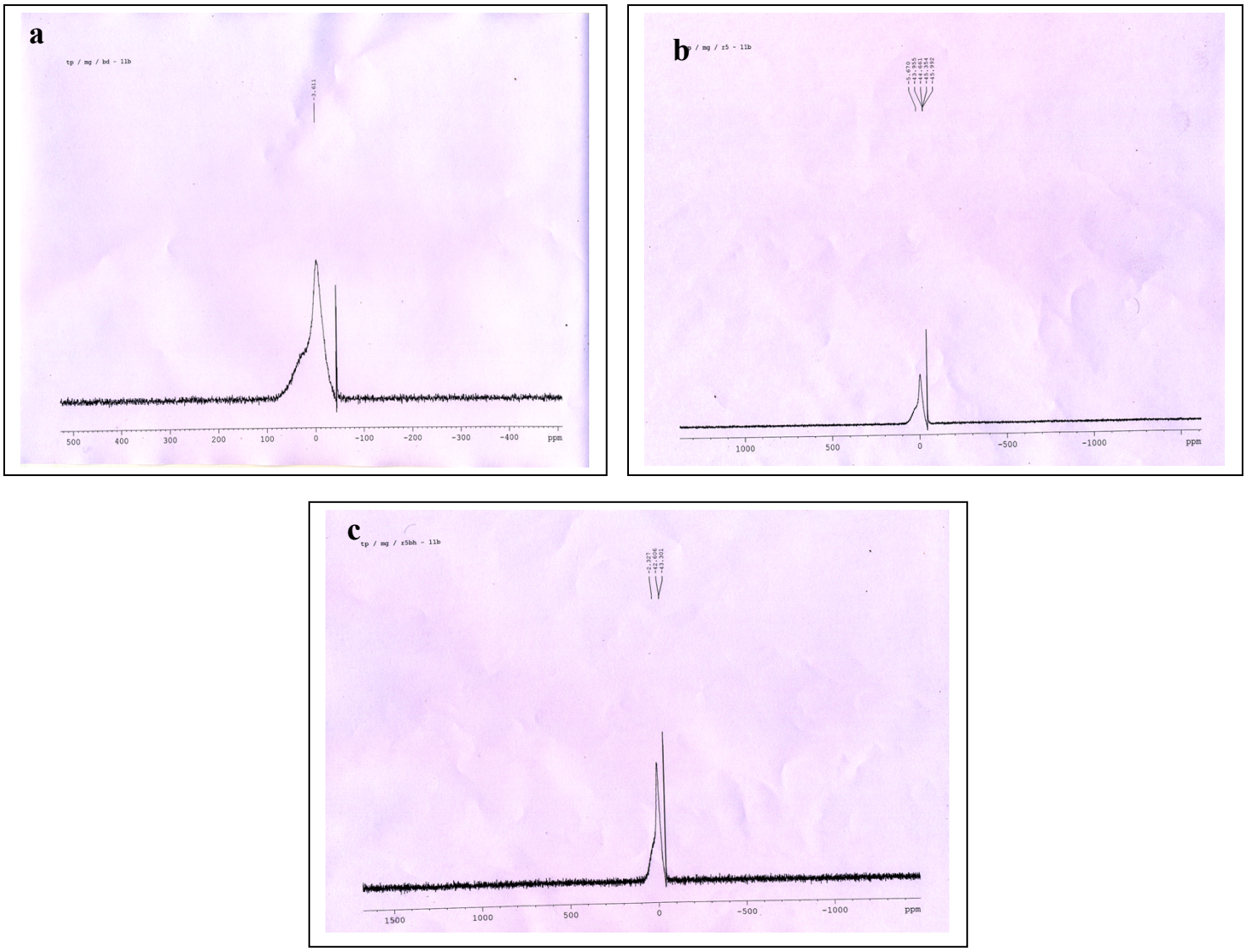

Figure S10: ^{11}B-NMR spectra of (a) $NaBH_4$ in d^8-THF, (b) PNA 2 in d^8-THF and (c) P-NA 3 (P-NA 2 + d^6-acetone) in d^8-THF

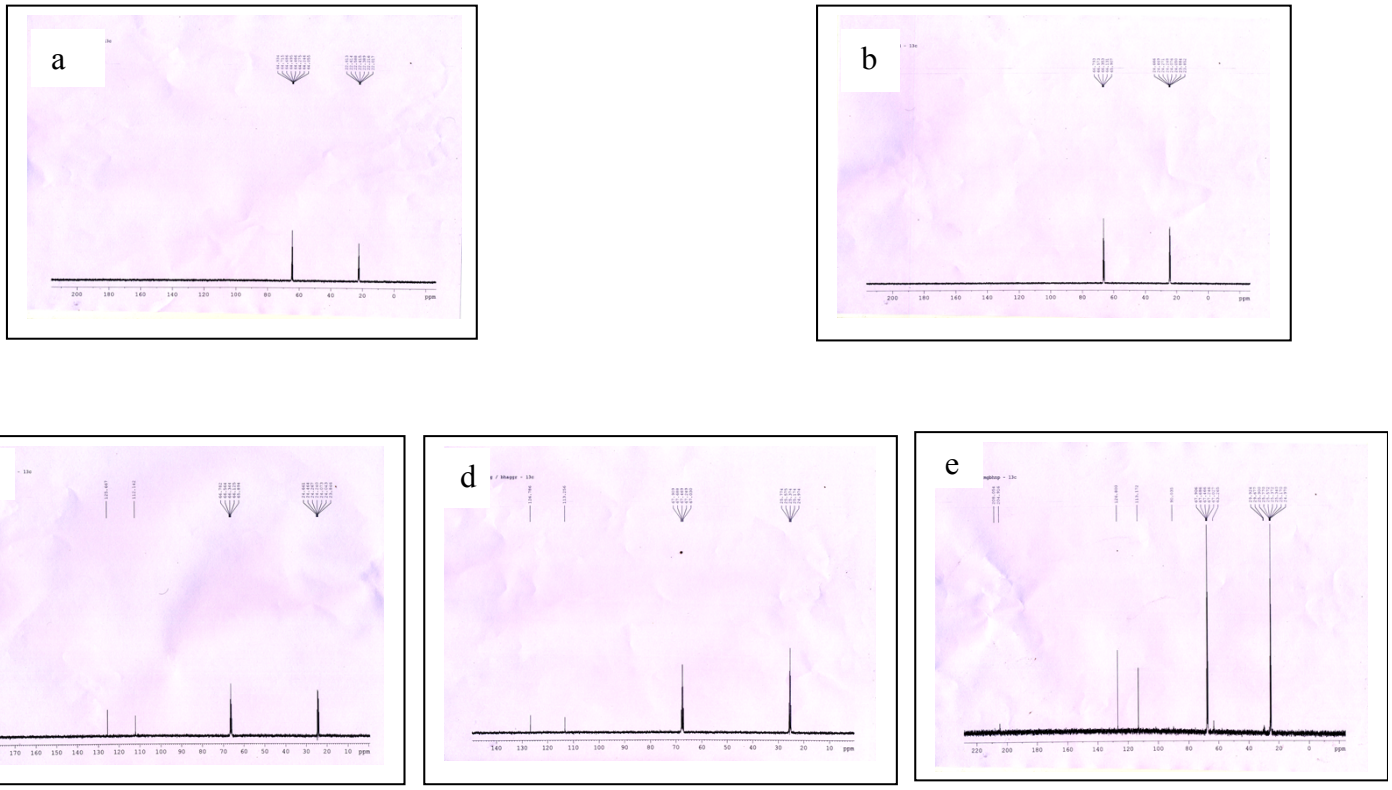

Figure S11: ^{13}C-NMR of (a) d^8-THF, (b) d^8-THF + $NaBH_4$, (c) P-NA 1 in d^8-THF and (d) P-NA 2 in d^8-THF and (e) P-NA 3 (P-NA 2 + d^6-acetone) in d^8-THF.

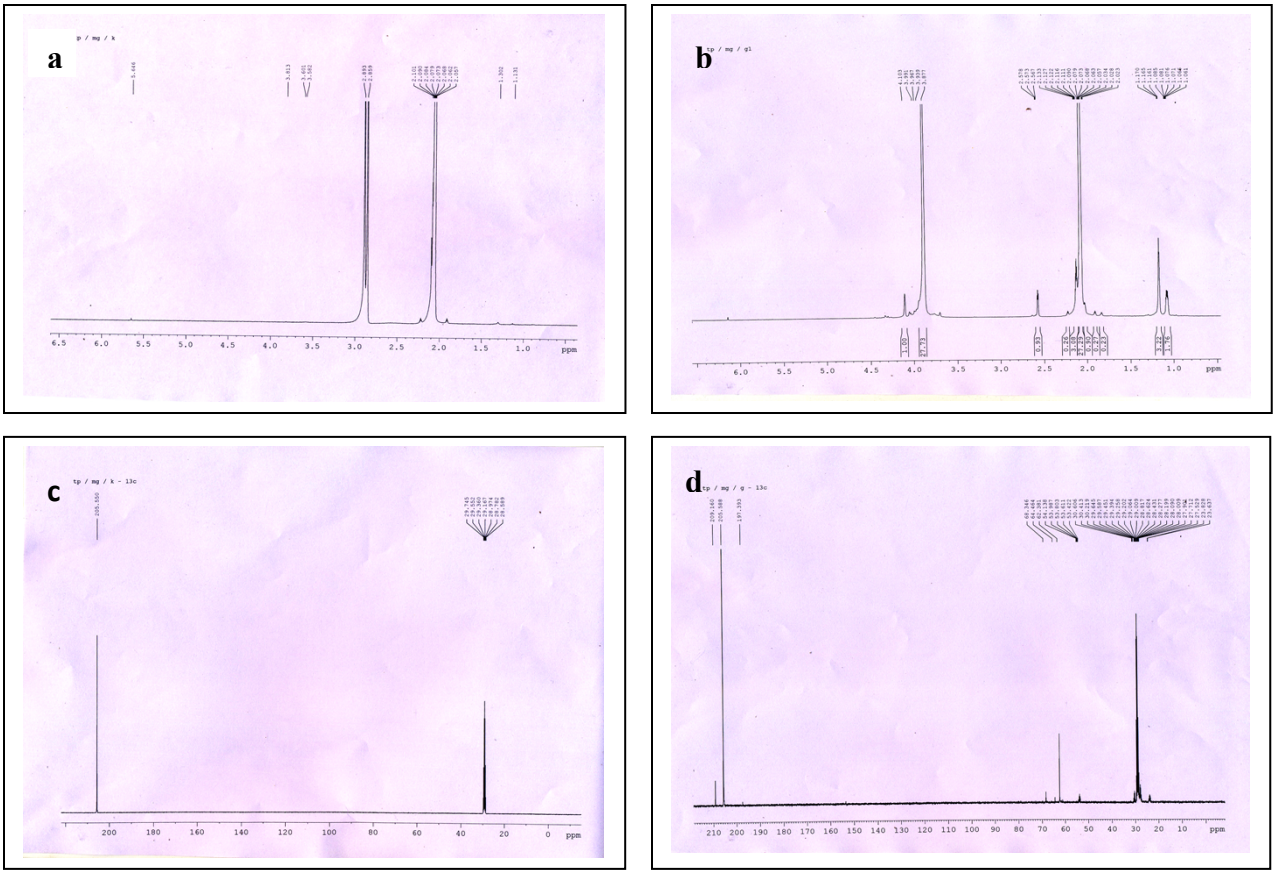

Figure S12: ^{1}H-NMR spectra of (a) acetone (b) acetone + sodium bohydride; ^{13}C-NMR spectra of (c) acetone (d) acetone + sodium bohydride.

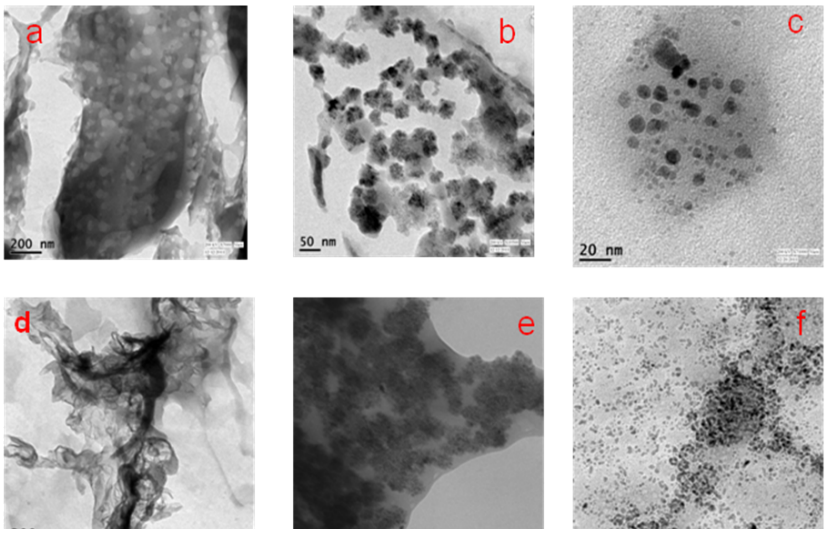

Figure S13: TEM image of (a) P-NA 1, (b) P-NA 2, (c) P-NA 3, (d) O-NA 1, (e) O-NA 2 and (f) O-NA 3. Condition: Nitroaniline conc. = 2.5 x 10^{-3} M, $NaBH_4$ conc. =3 x 10^{-2} M.

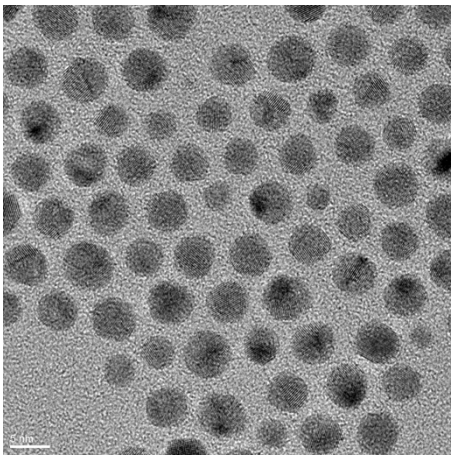

Figure S14: TEM image of dodecyl amine capped gold organosol.

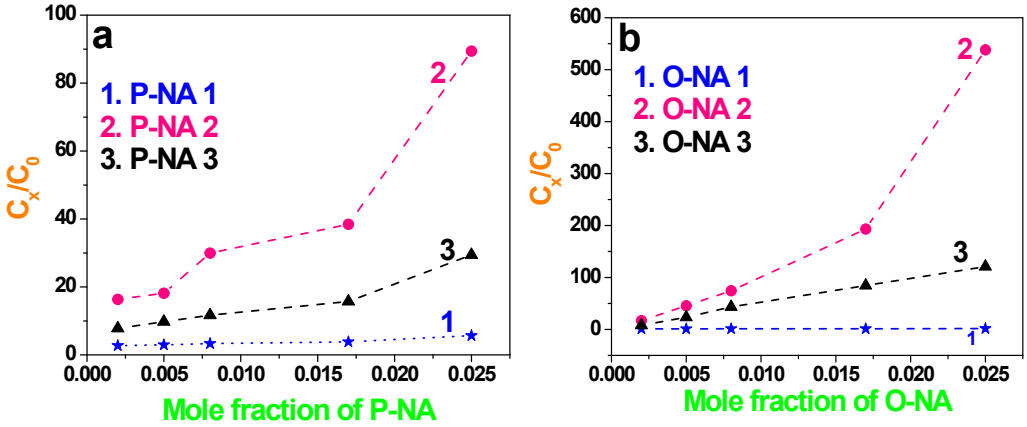

Figure S15: (a) Change of capacitance of (a) P-NA 1, P-NA 2, P-NA 3 with respect to pure THF at different mole fraction of para-nitroaniline and (b) O-NA 1, O-NA 2 and O-NA 3 with respect to pure THF at different mole fraction of ortho-nitroaniline.

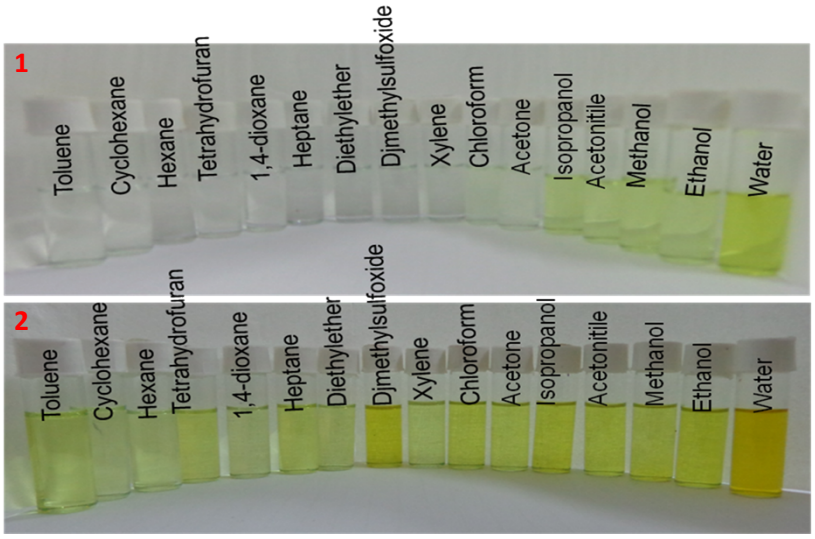

Figure S16: Digital image showing P-NA and O-NA in different solvents.

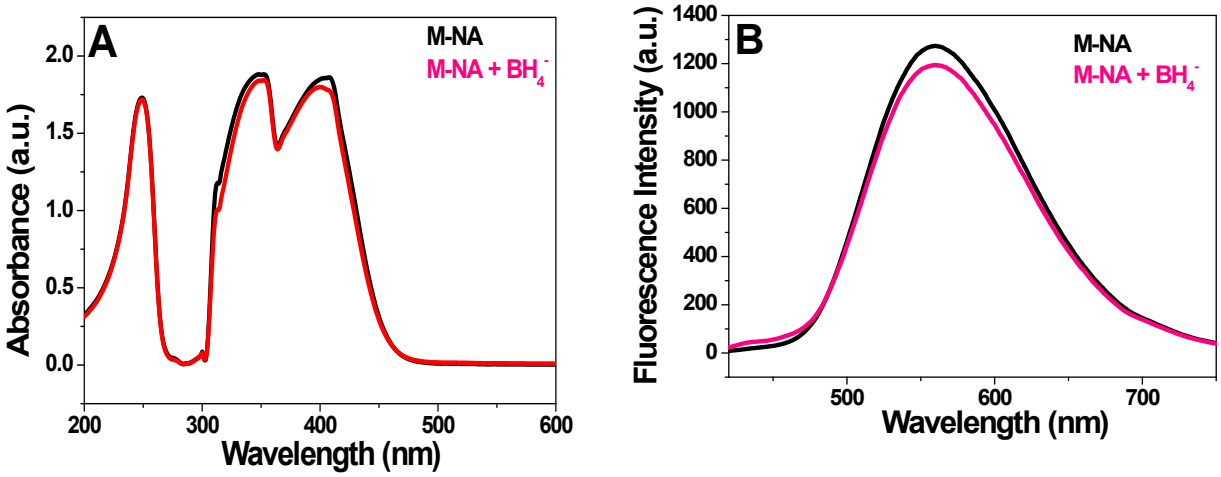

Figure S17: (A) UV-vis and (B) fluorescence spectra for the M-NA and M-NA /BH_4^- in THF. [M-NA] = 2.5×10^{-3} M, [BH_4^-] = 3.0×10^{-2} M.